Inorg. Chem. **2009**, *48*, 3581−3590

Influence of Conformational Flexibility on Self-Assembly and Luminescence Properties of Lanthanide Coordination Polymers with Flexible *exo*-Bidentate Biphenol Derivatives

Yanling Guo,[†] Wei Dou,[†] Xiaoyan Zhou,[†] Weisheng Liu,*[,†,‡] Wenwu Qin,[†] Zhipeng Zang,[†] Hongrui Zhang,[†] and Daqi Wang[§]

College of Chemistry and Chemical Engineering and State Key Laboratory of Applied Organic Chemistry, Lanzhou University, Lanzhou 730000, China, State Key Laboratory of Coordination Chemistry, Nanjing University, Nanjing 210093, China, and Department of Chemistry, Liaocheng University, Liaocheng 252000, China

Received October 27, 2008

To explore how nonplanar conformational distortions affect supramolecular self-assembly and properties of lanthanide complexes, we have designed and synthesized two new flexible exo-bidentate ligands derived from biphenol featuring two salicylamide pendant arms, 2,2′-bis{[(2′-benzylaminoformyl)phenoxyl]ethoxyl}-1,1′-biphenylene (L^{I}) and 5,5′-dibromo-2,2′-bis{[(2′-benzylaminoformyl)phenoxyl]ethoxyl}-1,1′-biphenylene (L^{II}). These two structurally related ligands can have different conformations and are used for constructing diverse lanthanide polymers with interesting luminescence properties. Among two series of lanthanide nitrate complexes which have been characterized by elemental analysis, X-ray powder diffraction, and IR spectroscopy, four new coordination polymers have been determined using X-ray diffraction analysis. The coordination polymer type $\{Ln_2(NO_3)_6(L^{I})_3 \cdot 3H_2O\}_\infty$ (Ln = Nd, Sm, Eu, Gd, Tb or Dy) displays a two-dimensional honeycomb-like framework in the *ab* plane, which can be regarded as a (6,3) topological network with neodymium atoms acting as "three-connected" centers. In contrast, the coordination polymer types $\{[Nd(NO_3)_3(L^{II})(CH_3OH)] \cdot CH_3OH\}_\infty$ and $[Ln(NO_3)_3(L^{II})(C_2H_5OH)]_\infty$ (Ln = Sm, Eu, Gd, Tb or Dy) possess single-stranded helix chains which can be further connected through intermolecular hydrogen bonds to form two-dimensional supramolecular sheets. The photophysical properties of trivalent Sm, Eu, Tb, and Dy complexes at room temperature were investigated. The present work substantiates the claim that the supramolecular structure as well as the luminescence properties of the coordination polymer can be tuned by controlling the conformational distortion of a nonplanar flexible ligand in the supramolecular self-assembly.

Introduction

The lanthanide complexes are noted for their unique luminescence properties arising from f−f transitions (including long excited-state luminescence lifetimes up to milliseconds, sharp transitions in the visible or in the near-infrared range with large Stokes shifts (>200 nm) and sensitivity to the local environment), which have made them one of the essential components in the preparation of new advanced materials.[1−3] The coordination polymers containing trivalent lanthanide ions (Eu^{3+}, Tb^{3+}) have attracted more and more attention, due to their promising applications in sensors, lighting devices, and optical storage.[4] However, the design and synthesis of highly luminescent coordination polymers with lanthanide-centered emission have been a

* To whom correspondence should be addressed. Tel.: +86-931-8915151. Fax: +86-931-8912582. E-mail: liuws@lzu.edu.cn.
† Lanzhou University.
‡ Nanjing University.
§ Liaocheng University.

(1) (a) Bünzli, J.-C. G.; Piguet, C. *Chem. Rev.* **2002**, *102*, 1897–1928. (b) Parker, D.; Dickins, R. S.; Puschmann, H.; Crossland, C.; Howard, J. A. K. *Chem. Rev.* **2002**, *102*, 1977–2010.
(2) (a) Richardson, F. S. *Chem. Rev.* **1982**, *82*, 541–552. (b) Pandya, S.; Yu, J.; Parker, D. *Dalton Trans.* **2006**, 2757–2766. (c) Beeby, A.; Botchway, S. W.; Clarkson, I. M.; Faulkner, S.; Parker, A. W.; Parker, D.; Williams, J. A. G. *J. Photochem. Photobiol. B* **2000**, *57*, 83–89. (d) Faulkner, S.; Pope, S. J. A.; Burton-Pye, B. P. *Appl. Spec. Rev.* **2004**, *39*, 1–35. (e) Yu, J.; Parker, D.; Pal, R.; Poole, R. A.; Cann, M. J. *J. Am. Chem. Soc.* **2006**, *128*, 2294–2299.
(3) Panigrahi, B. S. *Spectrochim. Acta, Part A* **2000**, *56*, 1337–1344.

10.1021/ic802060e CCC: $40.75 © 2009 American Chemical Society
Published on Web 03/16/2009

challenging task due to the influence of many factors upon the structures, such as the high coordination number and flexible coordination geometry of lanthanide metal ions and structural characteristics of polydentate organic ligands.[5−9] Novel lanthanide-based supramolecules with various topologies can be controlled and tuned through judiciously designing organic ligands as molecular building blocks.[10] So far, the various organic ligands used for constructing lanthanide coordination polymers are extensively derived from sulfoxides,[11] carboxylates,[12] pyridones,[13] nitrophenolate,[14] 4,4′-bipyridine-*N*,*N*′-dioxide,[15] and so on.[16] In particular, amide-type podand ligands provide a fascinating prospect in preparing lanthanide coordination polymers possessing strong luminescence properties,[7,17] which prompts us to investigate and synthesize analogues of the extensive series of ligands mentioned above.

Scheme 1. Structures of the Organic Ligands Used in This Work

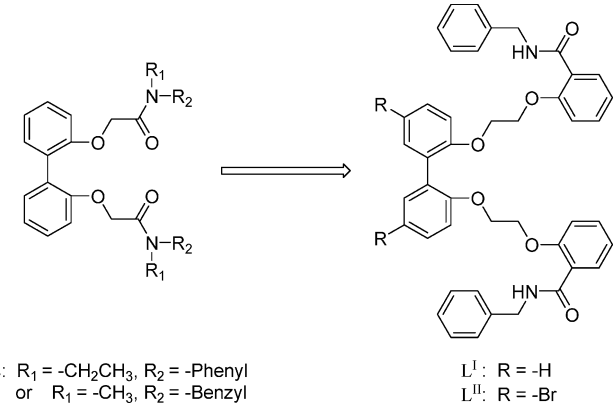

In our previous studies, considering that the configurations of ligands incorporating a biphenyl backbone can be greatly altered along the 1,1′ bond while the functional groups bind to the metal ions,[18] we have introduced a biphenyl connector into the reaction system and prepared a series of amide-type podand ligands (L) with various N-substituent groups (as shown in Scheme 1) and their rare earth complexes. We expected that the distortion of the biphenyl connector could endow the metal-organic frameworks with unique structural and functional properties. Unfortunately, all of the lanthanide complexes obtained so far represent simple chelate structures with all of the oxygen atoms of the ligands as donors bound to the lanthanide ions. In these complexes, the free rotation character of biphenyl and its influence on controlling supramolecular architectures have not been thoroughly demonstrated.[19,20] Therefore, we have designed and synthesized two new flexible exo-bidentate ligands incorporating a biphenyl skeleton bearing two arms of salicylamide moieties, 2,2′-bis{[(2′-benzylaminoformyl)phenoxyl]ethoxyl}-1,1′-biphenylene (L^{I}) and 5,5′-dibromo-2,2′-bis{[(2′-benzylaminoformyl)phenoxyl]ethoxyl}-1,1′-biphenylene (L^{II}), to extend our systemic research for the following reasons. First, flexible ligands containing exo-bidentate organic building blocks have been often used for the rational design of solid-state architectures of coordination polymers because of their

(4) (a) Sabbatini, N.; Guardigli, M.; Lehn, J.-M. *Coord. Chem. Rev.* **1993**, *123*, 201–228. (b) Piguet, C.; Bünzli, J.-C. G.; Bernardinelli, G.; Hopfgartner, G.; Petoud, S.; Schaad, O. *J. Am. Chem. Soc.* **1996**, *118*, 6681–6697. (c) Cahill, C. L.; de Lill, D. T.; Frisch, M. *CrystEngComm* **2007**, *9*, 15–26. (d) Hill, R. J.; Long, D. L.; Hubberstey, P.; Schröder, M.; Champness, N. R. *J. Solid State Chem.* **2005**, *178*, 2414–2419. (e) Bünzli, J. C. G.; Piguet, C. *Chem. Soc. Rev.* **2005**, *34*, 1048–1077. (f) Robin, A. Y.; Fromm, K. M. *Coord. Chem. Rev.* **2006**, *250*, 2127–2157.

(5) Yang, X.-P.; Su, C.-Y.; Kang, B.-S.; Feng, X.-L.; Xiao, W.-L.; Liu, H.-Q. *J. Chem. Soc., Dalton Trans.* **2000**, 3253–3260.

(6) Yang, X.-P.; Kang, B.-S.; Wong, W.-K.; Su, C.-Y.; Liu, H.-Q. *Inorg. Chem.* **2003**, *42*, 169–179.

(7) Sun, R.; Wang, S. N.; Xing, H.; Bai, J. F.; Li, Y. Z.; Pan, Y.; You, X. Z. *Inorg. Chem.* **2007**, *46*, 8451–8453.

(8) Liu, W.-S.; Jiao, T.-Q; Li, Y.; Liu, Q.; Tan, M. Y.; Wang, H; Wang, L. F. *J. Am. Chem. Soc.* **2004**, *126*, 2280–2281.

(9) Gao, H.-L.; Yi, L.; Zhao, B.; Zhao, X.-Q.; Cheng, P.; Liao, D.-Z.; Yan, S.-P. *Inorg. Chem.* **2006**, *45*, 5980–5988.

(10) (a) Su, C.-Y.; Cai, Y.-P.; Chen, C.-L.; Kang, B.-S. *Inorg. Chem.* **2001**, *40*, 2210–2211. (b) Ayyappan, P.; Evans, O. R.; Lin, W. B. *Inorg. Chem.* **2001**, *40*, 3328–3330. (c) Fan, J.; Zhu, H.-F.; Okamura, T.; Sun, W.-Y.; Tang, W.-X.; Ueyama, N. *Inorg. Chem.* **2003**, *42*, 158–162. (d) Cui, Y.; Ngo, H. L.; Lin, W. B. *Inorg. Chem.* **2002**, *41*, 5940–5942. (e) Chen, B. L.; Ma, S. Q.; Zapata, F.; Fronczek, F. R.; Lobkovsky, E. B.; Zhou, H.-C. *Inorg. Chem.* **2007**, *461*, 1233–1236.

(11) (a) Bu, X.-H.; Weng, W.; Chen, W.; Zhang, R.-H. *Inorg. Chem.* **2002**, *41*, 413–415. (b) Bu, X.-H.; Weng, W.; Du, M.; Chen, W.; Li, J.-R.; Zhang, R.-H.; Zhao, L.-J. *Inorg. Chem.* **2002**, *41*, 1007–1010. (c) Li, J. R.; Bu, X. H.; Zhang, R. H.; Duan, C. Y.; Wong, K. M. C.; Yam, V. W. W. *New J. Chem.* **2004**, *28*, 261–265. (d) Li, J. R.; Bu, X. H.; Zhang, R. H. *Inorg. Chem.* **2004**, *43*, 237–244. (e) Dalgarno, S. J.; Hardie, M. J.; Atwood, J. L.; Raston, C. L. *Inorg. Chem.* **2004**, *43*, 6351–6356.

(12) (a) Reineke, T. M.; Eddaoudi, M.; O'Keeffe, M.; Yaghi, O. M. *Angew. Chem., Int. Ed.* **1999**, *38*, 2590–2594. (b) Pan, L.; Adams, M. K.; Herandez, H. E.; Wang, X. T.; Zheng, C.; Hattori, Y.; Kaneko, K. *J. Am. Chem. Soc.* **2003**, *125*, 3062–3067. (c) Reineke, T. M.; Eddaoudi, M.; Moler, D.; O'Keeffe, M.; Yaghi, O. M. *J. Am. Chem. Soc.* **2000**, *122*, 4843–4844. (d) Guo, X. D.; Zhu, G. S.; Fang, Q. R.; Xue, M.; Tian, G.; Sun, J. Y.; Li, X. T.; Qiu, S. L. *Inorg. Chem.* **2005**, *44*, 3850–3855. (e) Daiguebonne, C.; Kerbellec, N.; Bernot, K.; Gérault, Y.; Deluzet, A.; Guillou, O. *Inorg. Chem.* **2006**, *45*, 5399–5406. (f) Qin, C.; Wang, X.-L.; Wang, E.-B.; Su, Z.-M. *Inorg. Chem.* **2005**, *44*, 7122–7129. (g) Zhang, Z.-H.; Okamura, T.; Hasegawa, Y.; Kawaguchi, H.; Kong, L.-Y.; Sun, W.-Y.; Ueyama, N. *Inorg. Chem.* **2005**, *44*, 6219–6227. (h) Marchal, C.; Filinchuk, Y.; Imbert, D.; Bünzli, J.-C. G.; Mazzanti, M. *Inorg. Chem.* **2007**, *46*, 6242–6244.

(13) (a) Goodgame, D. M. L.; Menzer, S.; Smith, A. M.; Williams, D. J. *Chem. Commun.* **1997**, 339–340. (b) Goodgame, D. M. L.; Hill, S. P. W.; Williams, D. J. *Inorg. Chim. Acta* **1998**, *272*, 131–140.

(14) Bürgstein, M. R.; Gamer, M. T.; Roesky, P. W. *J. Am. Chem. Soc.* **2004**, *126*, 5213–5218.

(15) (a) Long, D.-L.; Blake, A. J.; Champness, N. R.; Wilson, C.; Schröder, M. *J. Am. Chem. Soc.* **2001**, *123*, 3401–3402. (b) Long, D.-L.; Blake, A. J.; Champness, N. R.; Schröder, M. *Chem. Commun.* **2000**, 1369–1370.

(16) (a) Hagrman, P. J.; Hagrman, D.; Zubieta, J. *Angew. Chem., Int. Ed.* **1999**, *38*, 2638–2684. (b) Moulton, B.; Zaworotko, M. J. *Chem. Rev.* **2001**, *101*, 1629–1658. (c) Eddaoudi, M.; Moler, D. B.; Li, H.; Chen, B.; Reineke, T. M.; O'Keeffe, M.; Yaghi, O. M. *Acc. Chem. Res.* **2001**, *34*, 319–330. (d) Janiak, C. *Dalton Trans.* **2003**, 2781–2804.

(17) (a) Zhang, J.; Tang, Y.; Tang, N.; Tan, M.-Y.; Liu, W.-S.; Yu, K.-B. *J. Chem. Soc., Dalton Trans.* **2002**, 832–833. (b) Tang, Y.; Zhang, J.; Liu, W.-S.; Tan, M.-Y.; Yu, K.-B. *Polyhedron* **2005**, *24*, 1160–1166. (c) Song, X.-Q.; Liu, W.-S.; Dou, W.; Zheng, J.-R.; Tang, X.-L.; Zhang, H.-R.; Wang, D.-Q. *J. Chem. Soc., Dalton Trans.* **2008**, 3582–3591.

(18) (a) Wang, R. H.; Hong, M. C.; Luo, J. H.; Cao, R.; Weng, J. B. *Chem. Commun.* **2003**, 1018–1019. (b) Rueff, J.-M.; Pillet, S.; Claiser, N.; Bonaventure, G.; Souhassou, M.; Rabu, P. *Eur. J. Inorg. Chem.* **2002**, *89*, 5–900. (c) Kumagai, H.; Inoue, K.; Kurmoo, M. *Bull. Chem. Soc. Jpn.* **2002**, *75*, 1283–1289. (d) Wang, R.; Han, L.; Xu, L.; Gong, Y.; Zhou, Y.; Hong, M.; Chan, A. S. C. *Eur. J. Inorg. Chem.* **2004**, *375*, 1–3763.

(19) Guo, Y.-L.; Dou, W.; Wang, Y.-W.; Liu, W.-S.; Wang, D.-Q. *Polyhedron* **2007**, *26*, 1699–1710.

(20) Guo, Y.-L.; Wang, Y.-W.; Dou, W.; Zheng, J.-R.; Liu, W.-S.; Su, C.-Y. *Inorg. Chim. Acta* **2007**, *360*, 3361–3368.

flexibility and conformational freedom.[21] Second, the high extinction coefficients of ligand featuring salicylamide pendant arms in the near UV−vis range provide effective absorption of excitation energy, which promotes more effective energy transfer to the lanthanide ion.[22] Third, replacement of two hydrogen atoms in the 5- and 5′-positions of the biphenyl backbone by two relatively large bromine atoms may tune the conformational distortion of the ligand and markedly modify its coordination properties. What greatly interests us here is how the conformational distortions of nonplanar ligands impact the coordination and supramolecular motifs as well as the luminescence properties of lanthanide complexes based on the two structurally related ligands, which has been rarely reported in the literature.[23]

As a result, a series of novel coordination polymers derived from the two bridging ligands with structural variation from two-dimensional honeycomb-like (6,3) topological networks to one-dimensional single-stranded helical chains was isolated. Four compounds, namely, $[Nd_2(NO_3)_6(L^I)_3 \cdot 3H_2O]_\infty$ (**1**), $\{[Nd(NO_3)_3(L^{II})(CH_3OH)] \cdot CH_3OH\}_\infty$ (**2**), $[Eu(NO_3)_3(L^{II})(C_2H_5OH)]_\infty$ (**3**), and $\{[Tb(NO_3)_3(L^{II})(C_2H_5OH)] \cdot CH_3OH\}_\infty$ (**4**), were characterized via single-crystal X-ray diffraction analysis. The luminescence properties of the resulting complexes formed with Ln^{3+} (Ln = Sm, Eu, Tb, Dy) were also studied in detail.

Experimental Section

The Materials and Instrumentation section is given in the Supporting Information.

General Synthetic procedure for L^I and L^{II} (Scheme S1, Supporting Information). To a solution of N-benzylsalicylamide (4.09 g, 18 mmol) in dry DMF was added K_2CO_3 (2.50 g, 18 mmol), and afterward, the mixture was stirred and heated at 110 °C for 30 min. Then, a solution of 2,2′-bis(*p*-tosyloxyethoxyl)-1,1′-biphenylene (intermediate A) or 5,5′-dibromo-2,2′-bis(*p*-tosyloxyethoxyl)-1,1′-biphenylene (intermediate B) (6 mmol) in 15 mL of dry DMF was added dropwise to the above solution over 30 min. The resulting mixture was stirred and maintained at 110 °C for 8 h. After the reaction mixture was cooled to room temperature, distilled water (60 mL) was added, and the turbid solution was extracted with chloroform (3 × 40 mL). The combined organic phases were washed with water and dried with anhydrous Na_2SO_4. The solvent was removed under reduced pressure to give a crude product. The pure product was obtained using chromatography on silica gel or recrystallization.

2,2′-bis{[(2′-Benzylaminoformyl)phenoxyl]ethoxyl}-1,1′-biphenylene (L^I). Chromatography (0−15% ethyl acetate in petroleum ether gradient). Yield: 75%. Mp: 98.8−99.2 °C. Anal. calcd (found) for $C_{44}H_{40}N_2O_6$: C, 76.28 (76.51); H, 5.82 (5.76); N, 4.04 (4.88)%. IR (KBr, ν, cm^{-1}): 3394 (s, NH), 1650 (s, C═O), 1599 (m), 1532 (s), 1481 (m), 1296 (m), 1230 (s), 933 (m), 754 (s). ^1H NMR ($CDCl_3$, 300 MHz, ppm): δ 3.89 (t, J = 4.5 Hz, 4H, $-CH_2-$), 3.96 (t, J = 5.4 Hz, 4H, $-CH_2-$), 4.33 (d, J = 5.2 Hz, 4H, $NH-CH_2-$), 6.60 (t, J = 8.7 Hz, 4H, Ar−H), 6.84 (t, J = 6.9 Hz, 2H, Ar−H), 6.96 (t, J = 7.2 Hz, 2H, Ar−H), 7.02−7.23 (m, 16H, Ar−H), 7.88 (s, 2H, −NH−), 8.17 (d, J = 7.8 Hz, 2H, Ar−H). ^{13}C NMR ($CDCl_3$, 300 MHz, ppm): δ 43.68, 66.68, 67.37, 112.36, 112.80, 121.20, 121.42, 121.69, 127.00, 127.48, 127.98, 128.37, 128.58, 131.66, 132.07, 132.49, 138.34, 155.20, 156.38, 164.82. ESI-MS: m/z 693.3 ($M + H^+$).

5,5′-Dibromo-2,2′-bis{[(2′-benzylaminoformyl)phenoxyl]ethoxyl}-1,1′-biphenylene (L^{II}). Recrystallization from ethyl acetate. Yield: 68%. Mp: 131.6−133.0 °C. Anal. calcd (found) for $C_{44}H_{38}Br_2N_2O_6$: C, 62.13 (62.41); H, 4.50 (4.36); N, 3.09 (2.93)%. IR (KBr, ν, cm^{-1}): 3402 (s, NH), 1649 (s, C═O), 1600 (m), 1530 (s), 1481 (m), 1291 (m), 1226 (s), 936 (m), 754 (s). ^1H NMR ($CDCl_3$, 300 MHz, ppm): δ 3.93 (t, J = 3.9 Hz, 4H, $-CH_2-$), 4.06 (t, J = 3.6 Hz, 4H, $-CH_2-$), 4.48 (d, J = 5.4 Hz, 4H, $NH-CH_2-$), 6.53 (d, J = 9.0 Hz, 2H, Ar−H), 6.69 (d, J = 8.4 Hz, 2H, Ar−H), 7.05−7.35 (m, 18H, Ar−H), 7.87 (s, 2H, −NH−), 8.17 (dd, J = 8.1 Hz, 2H, Ar−H). ^{13}C NMR ($CDCl_3$, 300 MHz, ppm): δ 43.81, 66.82, 67.09, 112.24, 113.26, 114.07, 121.59, 121.73, 127.13, 127.42, 128.12, 128.39, 131.61, 132.17, 132.54, 133.96, 138.16, 154.18, 156.29, 164.79. ESI-MS: m/z 851.0 ($M + H^+$).

Synthesis of Lanthanide Nitrate Complex. To a clear solution of the ligand (0.1 mmol) in ethyl acetate (10 mL) was added lanthanide nitrate (0.10 mmol) in 2 mL of methanol or ethanol. The resulting solution was left stirring overnight at room temperature to afford a pale white solid, which was filtered off, washed three times with ethyl acetate, and dried in a vacuum over P_2O_5 for 24 h to give the analytically pure product in 60−75% yield. The complex was dissolved in a hot methanol/ethanol/ethyl acetate solution to make a concentrated solution in a round-bottom flask. Then, the flask was cooled, and the mixture was filtered into a sealed 25−40 mL glass vial for crystallization at room temperature. After about two weeks, crystals suitable for analysis were obtained. IR and elemental analysis data for all complexes are summarized in Table 1.

X-Ray Crystallography. The X-ray diffraction data were collected on a Bruker SMART 1000 CCD diffractometer operating at 50 kV and 30 mA using a graphite-monochromated Mo Kα radiation source (λ = 0.71073 Å). An empirical absorption correction based on a comparison of redundant and equivalent reflections was applied using SADABS. All of the structures were solved by direct methods and refined by full-matrix least-squares cycles on F^2. The coordinates of the non-hydrogen atoms were refined anisotropically, while hydrogen atoms were included in the calculation isotropically but not refined. The methylene and −NH of the benzylsalicylamide group in complex **2** are disordered and could not be completely modeled. The ethyl groups of the coordinating ethanol molecule in complexes **3** and **4** exhibit disorder over two positions and were modeled and refined successfully. Details of crystallographic parameters, data collection, and refinements for **1**−**4** are listed in Table 2; representative bond distances (Å) and angles (deg) are listed in Tables S1−S4 (Supporting Information).

Results and Discussion

Design and Synthesis of Ligands L^I and L^{II}. The fascinating coordination chemistry of luminescent lanthanide cations exhibited by salicylamide derivatives prompts us to expand further studies on the design and synthesis of new types of salicylamide ligands. As we know, the geometry of

(21) (a) Bu, X. H.; Chen, W.; Lu, S. L.; Zhang, R. H.; Liao, D. Z.; Bu, W. M.; Shionoya, M.; Brisse, F.; Ribas, J. *Angew. Chem., Int. Ed.* **2001**, *40*, 3201–3203. (b) Paz, F. A. A.; Khimyak, Y. Z.; Bond, A. D.; Rocha, J.; Klinowski, J. *Eur. J. Inorg. Chem.* **2002**, *282*, 3–2828. (c) Belcher, W. J.; Longstaff, C. A.; Neckenig, M. R.; Steed, J. W. *Chem. Commun.* **2002**, 1602–1603.

(22) (a) Zhao, Y; Tang, Y.; Liu, W.-S; Tang, N; Tan, M.-Y. *Spectrochim. Acta, Part A* **2006**, *65*, 372–377. (b) Li, Y.-F.; Tang, K.-Z.; Tang, Y.; Liu, W.-S.; Tan, M.-Y. *Spectrochim. Acta, Part A* **2008**, *71*, 1153–1157.

(23) Nurco, D. J.; Medforth, C. J.; Forsyth, T. P.; Olmstead, M. M.; Smith, K. M. *J. Am. Chem. Soc.* **1996**, *118*, 10918–10919.

Table 1. Elemental Analytical and IR Spectral Data for All Complexes

compound	elemental analysis (%)[a] C	H	N	Ln	IR (λ_{max}/cm^{-1}), ν(C=O)
$Nd_2L^I_3(NO_3)_6\cdot 3H_2O$	55.52 (55.65)	4.68 (4.74)	5.85 (5.90)	10.18 (10.13)	1610
$Sm_2L^I_3(NO_3)_6\cdot 3H_2O$	55.37 (55.41)	4.67 (4.72)	5.82 (5.87)	10.60 (10.51)	1612
$Eu_2L^I_3(NO_3)_6\cdot 3H_2O$	55.32 (55.35)	4.75 (4.72)	5.92 (5.87)	10.55 (10.61)	1611
$Gd_2L^I_3(NO_3)_6\cdot 3H_2O$	55.28 (55.14)	4.61 (4.70)	5.83 (5.85)	10.82 (10.94)	1611
$Tb_2L^I_3(NO_3)_6\cdot 3H_2O$	55.17 (55.08)	4.61 (4.69)	5.79 (5.84)	10.93 (11.04)	1610
$Dy_2L^I_3(NO_3)_6\cdot 3H_2O$	55.11 (54.94)	4.63 (4.68)	5.87 (5.82)	11.12 (11.26)	1615
$[NdL^{II}(NO_3)_3(CH_3OH)]\cdot CH_3OH$	44.47 (44.38)	3.65 (3.72)	5.59 (5.63)	11.46 (11.59)	1611
$[SmL^{II}(NO_3)_3C_2H_5OH]$	44.94 (44.81)	3.58 (3.60)	5.56 (5.68)	12.06 (12.19)	1610
$[EuL^{II}(NO_3)_3C_2H_5OH]$	44.83 (44.75)	3.62 (3.59)	5.72 (5.67)	12.28 (12.31)	1609
$[GdL^{II}(NO_3)_3C_2H_5OH]$	44.64 (44.56)	3.62 (3.58)	5.71 (5.65)	12.54 (12.68)	1612
$[TbL^{II}(NO_3)_3C_2H_5OH]$	44.62 (44.50)	3.64 (3.57)	5.72 (5.64)	12.71 (12.80)	1611
$[DyL^{II}(NO_3)_3C_2H_5OH]$	44.51 (44.37)	3.63 (3.56)	5.76 (5.62)	12.95 (13.05)	1613

[a] Data in parentheses are calculated values.

Table 2. Crystal Data and Structure Refinement Parameters for Polymers **1**−**4**

	1	**2**	**3**	**4**
empirical formula	$C_{132}H_{132}N_{12}O_{42}Nd_2$	$C_{46}H_{46}Br_2N_5O_{17}Nd$	$C_{46}H44Br_2N_5O_{16}Eu$	$C_{47}H_{48}Br_2N_5O_{17}Tb$
temp/K	294	293	298	298
M	2846.98	1244.94	1234.64	1273.64
cryst syst	monoclinic	monoclinic	monoclinic	monoclinic
space group	C_2/c	$P2(1)/n$	$P2(1)/n$	$P2(1)/n$
a/Å	35.6360(19)	13.013(7)	12.6969(11)	12.7677(13)
b/Å	23.5611(19)	22.404(12)	21.820(3)	21.930(3)
c/Å	22.6605(15)	18.865(10)	18.2704(18)	18.609(2)
β/deg	90.7780(10)	92.657(11)	92.629(2)	92.912(2)
V/Å^3	19025(2)	5494(5)	5056.4(9)	5203.6(10)
Z	4	4	4	4
D_{calcd}/kg m^{-3}	0.994	1.505	1.622	1.626
μ/mm^{-1}	0.601	2.469	2.893	2.969
F(000)	5856	2492	2464	2544
cryst size/mm	0.30 × 0.25 × 0.25	0.28 × 0.16 × 0.15	0.26 × 0.13 × 0.11	0.23 × 0.12 × 0.04
θ range for data collection/deg	1.73−25.50	1.81−25.25	1.91−25.00	1.44−25.00
index ranges, *hkl*	$-43 \le h \le 43$, $-27 \le k \le 28$, $-27 \le l \le 27$	$-15 \le h \le 15$, $-26 \le k \le 26$, $-22 \le l \le 20$	$-14 \le h \le 15$, $-25 \le k \le 19$, $-11 \le l \le 21$	$-14 \le h \le 15$, $-26 \le k \le 16$, $-18 \le l \le 20$
reflns collected/unique	48306/17446	27494/9921	21022/8749	21510/8675
data/restraints/params	17446/9/795	9921/190/644	8749/0/629	8675/0/647
goodness-of-fit on F^2	1.064	1.020	0.990	1.060
final R indices [$I > 2\sigma(I)$]	R1 = 0.0787, wR2 = 0.2032	R1 = 0.0712, wR2 = 0.1642	R1 = 0.0966, wR2 = 0.1832	R1 = 0.0947, wR2 = 0.1924
R indices (all data)	R1 = 0.1498, wR2 = 0.2489	R1 = 0.1800, wR2 = 0.2099	R1 = 0.2194, wR2 = 0.2002	R1 = 0.2683, wR2 = 0.2113

the organic ligands is an important issue in determining the framework structures. In our study, biphenyl was selected as the backbone with the aim of investigating effects of the distortion of the connector in the salicylamide-based ligands on the assembly process and products. Two salicylamide arms attached to the biphenyl group through a $-CH_2CH_2-$ spacer are rotationally free and are thus capable of adjusting to match the metal coordination preference. Such a divergent arrangement would favor the formation of coordination polymers instead of discrete complexes. The introduction of bromine atoms in the 5- and 5′- positions of the biphenyl backbone was used to slightly modulate the conformational distortion of the ligand and explore its influences on the supramolecular self-assembly as well as the luminescence properties of lanthanide complexes. As shown in Scheme 1, L^I and L^{II} were successfully obtained as pale white solids and are soluble in common organic solvents such as ethyl acetate, acetonitrile, $CHCl_3$, CH_3OH, and DMF. This potentially facilitates the solution reaction between the ligand and inorganic metal salts. The IR spectra of these ligands showed a −NH absorption stretch around 3400 cm^{-1}. The strong absorption stretch around 1650 cm^{-1} is consistent with carbonyl absorption, which is comparable to those corresponding bands in known compounds.

Structural Analysis of Lanthanide Complexes Based on Ligands L^I and L^{II}. Treatment of $Ln(NO_3)_3\cdot 6H_2O$ with the two ligands in an ethyl acetate−methanol or ethyl acetate−ethanol solution yields a series of complexes which, according to elemental analysis, IR, and X-ray powder diffraction (XRPD), exhibit similar structures and correspond to the formulas $Ln_2(NO_3)_6(L^I)_3\cdot 3H_2O$ (Ln = Nd, Sm, Eu, Gd, Tb, Dy), $Nd(NO_3)_3(L^{II})(CH_3OH)\cdot CH_3OH$, and $Ln(NO_3)_3(L^{II})(C_2H_5OH)$ (Ln = Sm, Eu, Gd, Tb, Dy), respectively. X-ray-quality crystals of $[Nd_2(NO_3)_6(L^I)_3\cdot 3H_2O]_\infty$ (**1**), $\{[Nd(NO_3)_3(L^{II})(CH_3OH)]\cdot CH_3OH\}_\infty$ (**2**), $[Eu(NO_3)_3(L^{II})(C_2H_5OH)]_\infty$ (**3**), and $\{[Tb(NO_3)_3(L^{II})(C_2H_5OH)]\cdot CH_3OH\}_\infty$ (**4**) were obtained after several weeks of slow evaporation of the ethyl acetate−methanol−ethanol solution in the air at room temperature. Complexation of the arms through the carbonyl functions is reflected in the ν(C=O) vibration, which is shifted toward lower energy by approximately 39 cm^{-1}. The complexes are soluble in DMF, DMSO, acetonitrile, ethanol, and methanol; slightly soluble in ethyl acetate and acetone; and insoluble in $CHCl_3$ and diethyl ether. To explore the other complex structures, with the exception of **1**, **2**, **3** and **4**, XRPD of those complexes was performed. The XRPD patterns (Figures S1 and S2, Supporting Information) of the other complexes showed the main reflections

remaining nearly identical with the samples **1**, **2**, **3**, and **4**, which confirmed that the two kinds of complexes have an isostructural relationship.

Crystal Structure of $\{[Nd_2(NO_3)_6(L^I)_3]\cdot 3H_2O\}_\infty$ (1). The single-crystal X-ray analysis reveals that complex **1** crystallizes in monoclinic space group C_2/c and possesses a porous 2-D honeycomb open framework constructed from an extended array of trigonal-pyramidal Nd^{3+} centers and exo-bidentate L^I ligands. L^I molecules act as bridging linkers through their carbonyl oxygen atoms. The asymmetric unit in **1** contains one crystallographically independent Nd^{3+} center such that all of the Nd^{3+} centers are crystallographically equivalent. As shown in Figure 1a, the coordination sphere around each Nd^{3+} center consists of six oxygen atoms coming from three bidentate nitrate groups (O4, O5, O7, O8, O10, and O12) and three oxygen atoms coming from three salicylamide moieties of three separate L^I ligands (O3, O13, and O18). The coordination environment of nine oxygen atoms around the Nd^{3+} center can be described as a distorted monocapped square antiprism. The Nd−O(nitrate) bond lengths span the range of 2.524(5)−2.562(5) Å, but the Nd−O(carbonyl) bond lengths vary from 2.375(5) to 2.412(5) Å, both of which are comparable to the corresponding Nd−O(carbonyl) bond lengths found in related complexes.[24] At the same time, each L^I ligand acts as an exo-bidentate linker and binds to two Nd^{3+} centers using its two carbonyl oxygen atoms of the amide groups. Thus, each L^I ligand is coordinated to two Nd^{3+} and each Nd^{3+} is coordinated to three L^I ligands to form a 3:2 complex. Six L^I linkers alternately bridge six $Nd(NO_3)_3$ moieties to form a chair-conformational hexagonal 126-membered ring, in which three nonadjacent neodymium atoms are coplanar, paralleling the remaining three nonadjacent neodymium atoms with a plane-to-plane distance of 11.899 Å. The hexagonal rings are edge-sharing to each other, yielding a 2-D honeycomb-like framework in the *ab* plane (Figure 1b), which can be regarded as a (6,3) topological network with neodymium atoms acting as "three-connected" nodes and $Nd(L^I)_{3/2}(NO_3)_3$ units being regarded as repeating units. All of the counterions, NO_3^-, do not lie in cavities within the network but bind to the Nd^{3+} centers. This makes the framework a completely neutral network.

Seen from the crystal structure of **1**, the layers stack together parallel to the *c* axis, and no self-interpenetration of networks is observed, which should be avoided in view of constructing molecular-based microporous materials. Moreover, one-dimensional channels along the *c* axis are formed, which are occupied by the lattice water molecules (Figure 1c). The internal dimensions of the channel which have been evaluated taking into account the van der Waals radii of the involved atoms are about 9.5 × 13 Å. Calculations using PLATON[25] reveal that the solvent-accessible portion accounts for about 33% of the crystal volume. This dimension is sufficient to recognize suitable aromatic guest

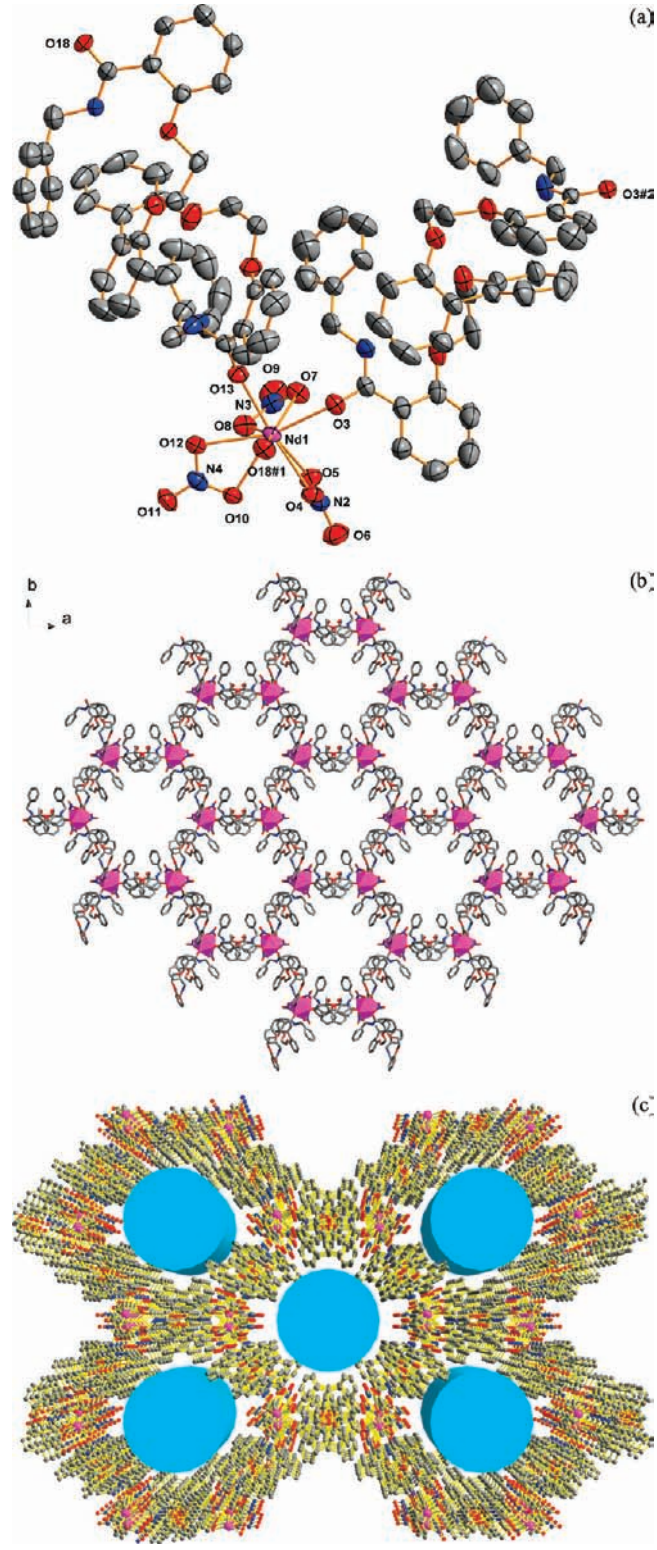

Figure 1. (a) Structure of of $Nd(NO_3)_3(L^I)_2$ showing the coordination sphere of Nd^{3+} in complex **1** along with atom labeling schemes and 30% thermal ellipsoids. Hydrogen atoms and crystal lattice water molecules are omitted for clarity. (The symmetry codes are #1 = $-x + 1/2$, $y - 1/2$, $-z + 1/2$; #2 = $-x + 1$, y, $-z + 1/2$.) (b) View of the 2-D honeycomb (6,3) topology network of complex **1** in the *ab* plane (hydrogen atoms and crystalline water molecules are omitted for clarity). (c) View of 2-D noninterpenetrating honeycomb-like layers of (6,3) topology with 1-D channels along the *c* axis (hydrogen atoms as well as crystalline water molecules are omitted for clarity). The blue insets show the 1-D perforative columnlike channels.

(24) Song, X.-Q.; Zhou, X.-Y.; Liu, W.-S.; Dou, W.; Ma, J.-X.; Tang, X.-L.; Zheng, J.-R. *Inorg. Chem.* **2008**, *47*, 11501–11513.
(25) Spek, A. L *PLATON*; Utrecht University: Utrecht, The Netherlands, 2003.

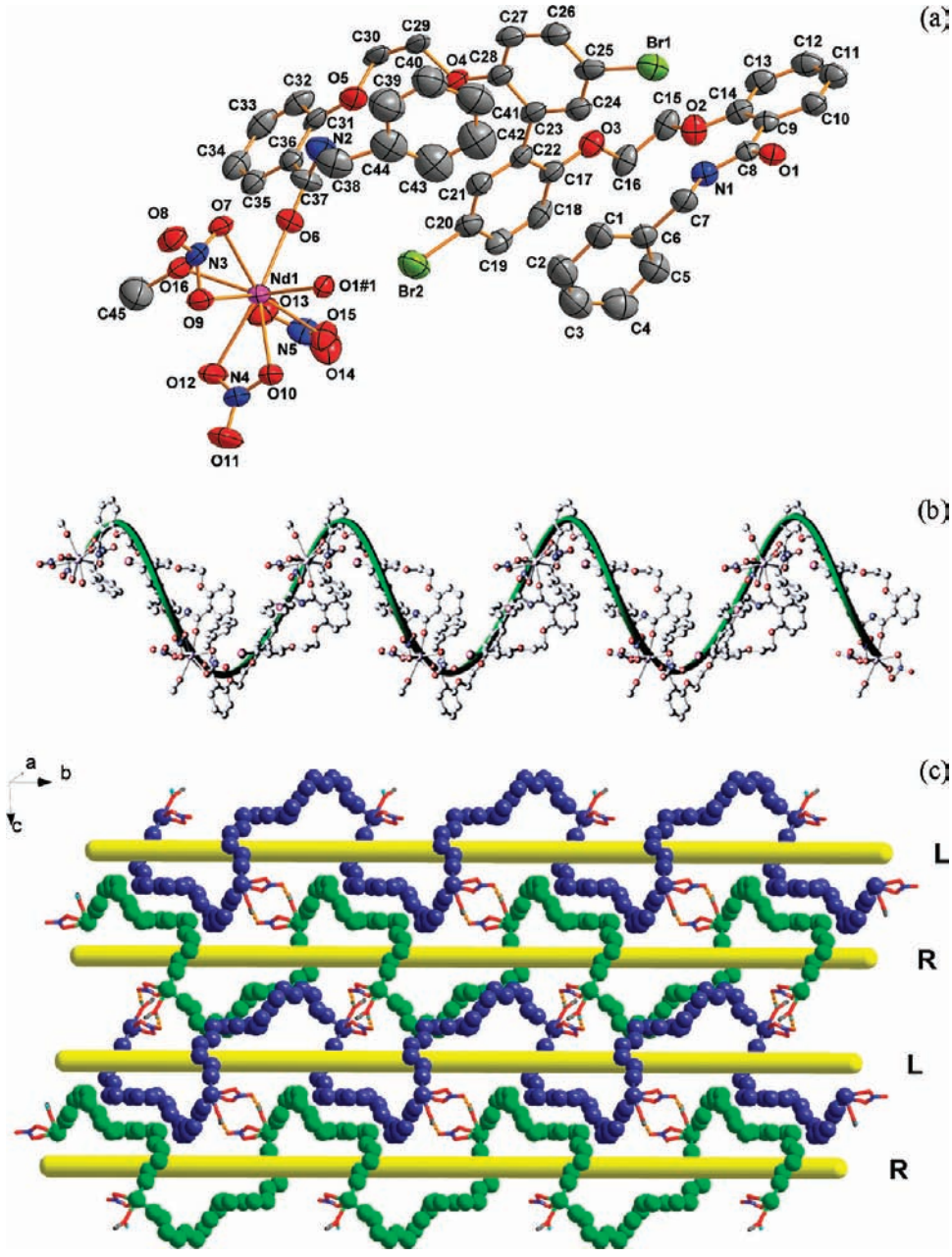

Figure 2. (a) Structure of $[Nd(NO_3)_3(L^{II})(CH_3OH)]$, showing the coordination sphere of Nd^{3+} in complex **2** along with atom numbering scheme and 30% thermal ellipsoids. For clarity, hydrogen atoms and crystal lattice solvent (methanol) are omitted. Only one set of atoms for each of the disordered $-CH_2NH$ groups is shown. (The symmetry code is #1 = $-x + 3/2$, $y - 1/2$, $-z + 3/2$.) (b) View of the 1-D infinite neutral coordination single-strand helix of the Nd^{3+} complex with L^{II} ligand along the *b* axis (hydrogen atoms and crystalline water molecules are omitted for clarity). (c) View of the 2-D supramolecular sheet of **2** constructed by bridging the alternate left-handed (indigo) and right-handed (bright green) helical chains through intermolecular O16−H6···O8 hydrogen bonds [symmetry code is $2 - x$, $-y$, $1 - z$; and the hydrogen bonds are indicated by the light-orange dashed lines] (some atoms of the ligand and nitrates and crystalline methanol molecules are omitted for clarity).

molecules. Note that the channel walls of **1** are full of oxygen atoms; such crown-ether-like channels are of considerable interest in the broader scientific context. To the best of our knowledge, this type of non-interpenerating neutral (6,3) topological framework with large macrometallocycles constructed by linking flexible amide podands with rare earth ions is unprecedented.

Crystal Structure of $\{[Nd(NO_3)_3(L^{II})(CH_3OH)]\cdot CH_3OH\}_\infty$ (2). Slight structural modification involving introduction of bromine atoms in the 5- and 5′- positions of the biphenyl backbone was applied in the synthesis of L^{II}, which was used instead of L^{I} to perform the reaction with lanthanide nitrates. Compounds **2**, **3**, and **4** were obtained as crystals by the reaction of L^{II} with $Ln(NO_3)_3\cdot 6H_2O$ in an ethyl acetate−ethanol−methanol system. The single-crystal X-ray analysis reveals that they possess the same topological structures despite the fact that a coordinated methanol molecule that occurs in **2** was replaced by a coordinated ethanol molecule in **3** and **4**. Thus, only **2** is selected for investigation here in detail as a representative example. Complex **2** crystallizes in monoclinic space group *P*2(1)/*n*, and the asymmetric unit contains one crystallographically independent Nd^{3+} center. As shown in Figure 2a, each Nd^{3+} center is surrounded by two carbonyl oxygen atoms coming

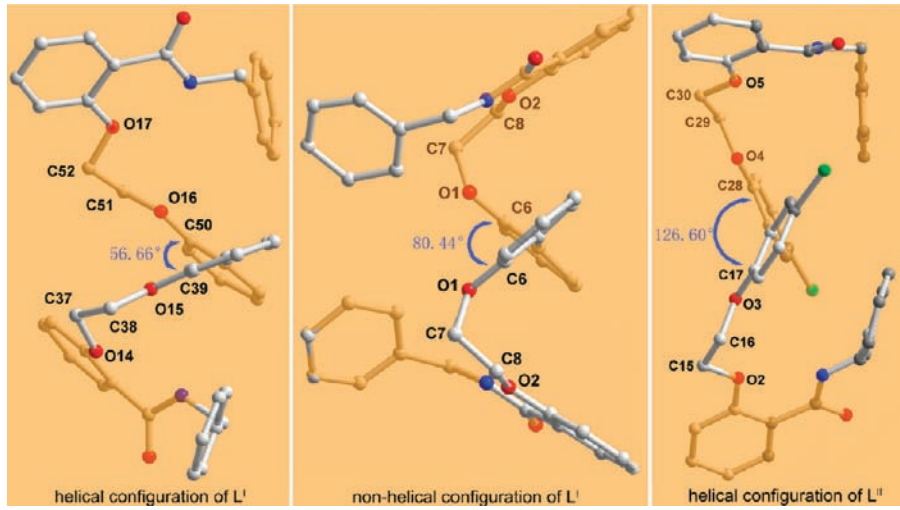

Figure 3. View of the conformations of ligands L^I in complex **1** and L^{II} in complex **2**.

from two salicylamide moieties of different L^{II} ligands (O1 and O6), six oxygen atoms coming from three bidentate nitrate groups (O7, O9, O10, O12, O13, and O15), and one oxygen atom provided by the coordinate methanol molecule (O16). The coordination environment of nine oxygen atoms around the Nd^{3+} center can be best described as a slightly distorted monocapped square antiprism. The Nd−O(nitrate) bond lengths span the range of 2.371(7)−2.399(7) Å, the Nd−O(carbonyl) bond lengths vary from 2.510(8) to 2.615(9) Å, and the Nd−O(methanol) bond length corresponds to 2.493(7) Å, all of which are comparable with those observed in other Nd^{3+}-containing coordination polymers. Each Nd^{3+} is coordinated to two L^{II} ligands; each L^{II} ligand behaves in an exo-bidentate mode bridging a pair of adjacent Nd^{3+} centers (O1 for one Nd^{3+} and O6 for the other Nd^{3+}). Thus, each L^{II} ligand is coordinated to two Nd^{3+} ions and each Nd^{3+} is coordinated to two L^{II} ligands to form a 1:1 complex. The interconnections of the L^{II} ligands and the nine-coordinate Nd^{3+} centers form a one-dimensional, infinite neutral coordination single-stranded helical chain (Figure 2b) with a Nd−Nd−Nd internal angle of 91.19°, which is obviously different from the (6,3) topological network of complex **1**. The repeating period in the helical chain contains two Nd−L^{II} units. The helical pitch, given by the distance between equivalent atoms generated by one full rotation of the 2-fold screw axis, is 22.404 Å, which is obviously longer than the Nd···Nd distance of 15.680 Å bridged by the L^{II} ligand. One-dimensional left-hand and right-hand helical chains are alternatively connected, via the significant supramolecular hydrogen bond O16−H6···O8 [O8···H6, 1.9510 Å and O16−H6···O8#1, 176.53°; symmetry code #1: $2 - x, -y, 1 - z$] formed among the coordinated methanol oxygen atoms and nitrate groups, to further generate a unique two-dimensional supramolecular sheet structure (Figure 2c). It should be noted that examples of one-dimensional single-helical chains constructed by linking biphenyl derivative ligands with Ln^{3+} ions remain limited according to the literature.

Conformation Analysis of the Two Ligands in Their Complexes. To understand the conformational distortions of ligands that influence the assembly topological architectures in **1** and **2** in more detail, a conformation analysis of ligands L^I and L^{II} is presented. As shown in Figure 3, the two crystallographically independent L^I ligands in **1** adopt the helical and nonhelical conformations, respectively, whose assembly with metal ions produces an unusual framework. The dominant conformation found for ligand L^I in the X-ray molecular structure is helical and allows its two salicylamide arms to stretch out. Moreover, it acts as a middle spacer with a shortest O···O distance of 13.043 Å between the two carbonyl oxygen donor atoms. The distortion angles of O14−C37−C38−O15,O16−C51−C52−O17,C37−C38−O15−C39, and C50−O16−C51−C52 are 65.84, 67.84, 171.25, and 168.14°, respectively. The relatively smallest twisting is observed between the two phenyl rings about the 1,1′ bond, with a dihedral angle of 56.66°. The portion of the ligand L^I featuring nonhelical conformation is arranged with its two salicylamide arms in a gathered-round fashion and acts as a shorter spacer, with a shortest O···O distance of 12.175 Å between the two carbonyl oxygen donor atoms. In this type of L^I ligand, there is a C_2 symmetrical axis which is perpendicular to the 1,1′ bond and crosses the center of the 1,1′ bond. It is worth noting that the distortion fashion of the $-CH_2CH_2-$ groups is significantly different from that observed in the L^I ligand featuring helical configuration (φO2−C8−C7−O1 = −63.49° and φC8−C7−O1−C6 = −68.28°), which is considered to play the dominant role in determining the conformation adopted by the ligand. A middle twisting is observed between the two phenyl rings about the 1,1′ bond, with a dihedral angle of 80.44°. However, **2** contains only one crystallographically independent L^{II} ligand, which adopts the helical conformation rather than the nonhelical conformation, appearing largely as a consequence of the steric factor. Each L^{II} ligand in **2** acts as a longer spacer, with a shortest O···O distance of 13.339 Å

(26) Borgne, T. L.; Bénech, J.-M.; Floquet, S.; Bernardinelli, G.; Alipprandini, C.; Bettens, P.; Piguet, C. *J. Chem. Soc., Dalton Trans.* **2003**, 3856–3868.

between the two carbonyl oxygen donor atoms. The O···O distance of the L^{II} ligand is much longer than those of L^{I} ligands in **1**, indicating that the L^{II} ligand in complex **2** has a more extended conformation. The distortion fashion of the $-CH_2CH_2-$ groups is similar to that observed in the L^{I} ligand featuring helical conformation (φO5−C30−C29−O4 =71.38°,φO3−C16−C15−O2=68.74°,φC30−C29−O4−C28 = 173.97°, φC17−O3−C16−C15 = 176.61°). It is worth pointing out that the relatively largest twisting is observed between the two brominated phenyl rings about the 1,1′ bond, with a dihedral angle of 126.60°, which is much larger than those observed in **1**. The possible explanation for this change might be that such an arrangement may reduce the steric hindrance and make the whole framework more stable. In fact, the ligands in **2**, **3**, and **4** were arranged in a virtually identical fashion with minor differences due to slight changes in folding at $-CH_2CH_2-$ groups or small rotations of C−C bonds.

The coordinative behavior of the ligand indicates that the conformational distortion of this type of ligand can be modulated by introducing two bromine atoms in the 5- and 5′- positions of the biphenyl backbone. The alteration of the ligand conformations along with the relative orientations of the salicylamide arms are responsible for the distortion fashion of the $-CH_2CH_2-$ groups, the O···O distances, and the dihedral angles between the phenyl rings provided by the biphenyl unit. Compared with L^{I} in **1**, the conformational distortion of L^{II} in **2** is significantly changed due to the presence of two relatively large bromine atoms, which induces the dramatic twisting of the biphenyl and more extended orientations of the salicylamide arms to reduce the steric hindrance. On the other hand, the introduction of two relatively large bromine atoms in the 5- and 5′- positions of the biphenyl backbone has obviously increased the steric demand of the L^{II} ligand, although it has not affected the coordinative mode of the functional terminal groups. Because of the significant steric congestion, one metal center is limited to coordination with two functional groups of two separate L^{II} ligands rather than three in the self-assembly process, thus leading to the formation of the 1:1 (L/M) complex of L^{II}, which is quite different from the 3:2 (L/M) complex of L^{I}.[26] Consequently, the two-dimensional honeycomb-like (6,3) topological network of the complex with L^{I} degrades to the one-dimensional single-stranded helical chain of complex with L^{II}.

Luminescence Properties of Ligands and their Complexes in the Solid State. Upon UV irradiation, the free ligands emit a strong blue luminescence (apparent λ_{max} at ca. 457 nm for L^{I} and ca. 468 nm for L^{II}). However, upon complexation, this emission is replaced by the corresponding lanthanide cation emitting in the visible range (Sm^{3+}, Eu^{3+}, Tb^{3+}, and Dy^{3+}), which can be readily seen with the naked eye, indicating the occurrence of ligand-to-metal intramolecular photoinduced energy transfer.

The solid-state excitation and emission spectrum of the Eu^{3+} complex of L^{I} at room temperature is shown in Figure 4, and the relevant photophysical data are summarized in Table 3. The excitation spectrum of the Eu^{3+} complex of L^{I} has negligible contributions from the ligand and exhibits a series of sharp lines characteristic of the Eu^{3+} energy-level structure that can be assigned to transitions between the $^7F_{0,\,1}$ and the $^5L_6$ and $^5D_{2,\,1}$ levels.[27] This indicates that luminescence sensitization of the Eu^{3+} complex via excitation of the ligand is not efficient. The ambient-temperature emission spectrum of the Eu^{3+} complex is characteristic of the metal in the 550−700 nm region, with well-resolved transitions that are anticipated from the metal-centered $^5D_0$ excited state to the ^7F_J ground-state multiplet. Maximum intensities at 580, 593, 617, 652, and 694 nm, respectively, were observed for the $J = 0$, 1, 2, 3, and 4 transitions, and the $J = 2$ so-called "hypersensitive" transition is extremely intense. The intensity of the $^5D_0 \rightarrow {}^7F_2$ transition (electric dipole) is stronger than that of the $^5D_0 \rightarrow {}^7F_1$ transition

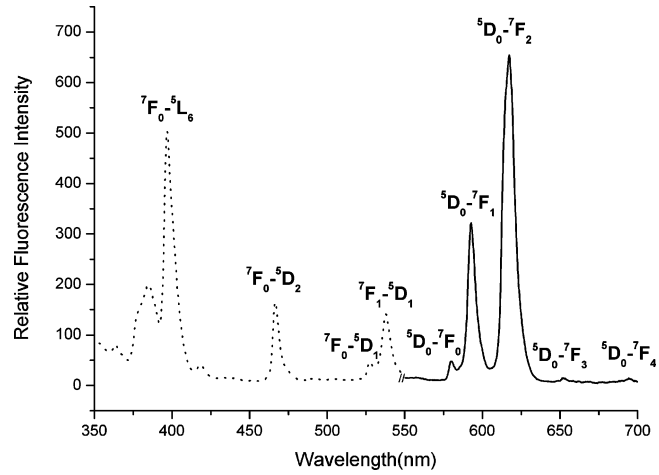

Figure 4. Room-temperature excitation and emission spectra for the Eu^{3+} complex of ligand L^{I} (λ_{ex} = 396 nm, excitation and emission passes = 2.5 nm) in the solid state with emission monitored at approximately 617 nm.

Table 3. Photophysical Characterization of the L^{I} and L^{II} Complexes

		λ_{max}[a]/nm	RFI/au	τ/ms	Φ[b] (%)
L^{I}	Sm	564	97	0.061	0.73
		598	127		
	Eu	580	48		
		593	321		
		617	654	1.108	10.36
		652	14		
		694	13		
	Tb	492	>10 000		
		546	>10 000	1.599	29.76
		583	2863		
		621	1064		
	Dy	484	1659	0.073	5.58
		574	1371		
L^{II}	Sm	562	40	0.010	0.21
		597	41		
	Eu	593	148		
		619	405	0.573	2.97
	Tb	492	2737		
		545	6771	1.155	7.41
		585	348		
	Dy	483	690	0.014	0.43
		574	614		

[a] Excitation and emission passes = 2.5 nm. [b] Luminescence lifetimes and quantum yield values are reported here with an error of ±15%.

(27) (a) Shyni, R.; Biju, S.; Reddy, M. L. P.; Cowley, A. H.; Findlater, M. *Inorg. Chem.* **2007**, *46*, 11025–11030. (b) Biju, S.; Raj, D. B. A.; Reddy, M. L. P.; Kariuki, B. M. *Inorg. Chem.* **2006**, *45*, 10651–10660.

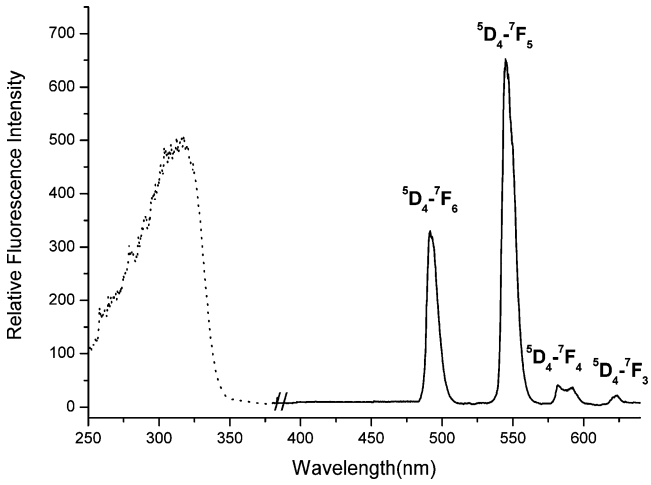

Figure 5. Room-temperature excitation and emission spectra for the Tb^{3+} complex of ligand L^I ($\lambda_{ex} = 317$ nm, excitation and emission passes = 1.0 nm) in the solid state.

(magnetic dipole), which indicates that the coordination environment of the Eu^{3+} ion is asymmetric.[28] The fluorescence quantum yield, ϕ, of the Eu^{3+} complex in the solid state was found to be 10.36% using an integrating sphere. The solid-state luminescence lifetime value for the $^5D_0$ level of the Eu^{3+} complex was determined to be 1.108 ms from the luminescence decay profile at room temperature by fitting with a monoexponential curve (Figure S6, Supporting Information).

For the Tb^{3+} complex of L^I, the excitation spectrum monitored characteristic emission of Tb^{3+} ion in the solid state (Figure 5) overlaps the absorption spectrum in the 250−340 nm region, indicating a very efficient energy transfer from the ligand to the Tb^{3+} center. The room-temperature normalized emission spectrum of the Tb^{3+} complex exhibits the characteristic emission bands for Tb^{3+} centered at 490, 545, 585, and 620 nm, shown in Figure 5, which result from deactivation of the $^5D_4$ excited state to the corresponding ground state ^7F_J ($J = 6, 5, 4, 3$) of the Tb^{3+} ion. The most-intense emission is centered at 545 nm and corresponds to the hypersensitive transition $^5D_4 \rightarrow {}^7F_5$. The fluorescence quantum yield, ϕ, of the Tb^{3+} complex in the solid state was found to be 29.76% using an integrating sphere. The solid-state luminescence lifetime value for the $^5D_4$ level of the Tb^{3+} complex was determined to be 1.599 ms from the luminescence decay profile at room temperature by fitting with a monoexponential curve (Figure S7, Supporting Information).

The potential for antenna-modified ligand L^I to sensitize other visible emitting lanthanide cations, notably Sm^{3+} and Dy^{3+}, was also evaluated. For the Sm^{3+} complex of L^I, two characteristic bands can be observed, which are attributed to $^4G_{5/2} \rightarrow {}^6H_J$ ($J = 5/2, 7/2$) transitions (Figure S4, Supporting Information). In the case of Dy^{3+}, two characteristic narrow bands can be seen in the emission spectrum, which are attributed to transitions of 483 nm ($^4F_{9/2} \rightarrow {}^6H_{15/2}$) and 574 nm ($^4F_{9/2} \rightarrow {}^6H_{13/2}$) (Figure S5, Supporting Information). Quantum yield measurements for the Sm^{3+} and Dy^{3+} complexes in the solid state were found to be 0.73 and 5.58, respectively, using an integrating sphere. The luminescence decays are best described by a single-exponential process with lifetimes of 0.061 ms for the Sm^{3+} complex and 0.073 ms for the Dy^{3+} complex.

Furthermore, the normalized emission spectra for the four complexes of L^{II} were recorded. The relevant photophysical data (Figures S8−S9, Supporting Information) are summarized in Table 3.

In contrast to the complexes of L^I, the intensities of the four complexes of L^{II} are relatively weak; the corresponding quantum yields and lifetimes are also relatively small and short, indicating the presence of one or more nonradiative deactivation pathway to the excited state. Because the triplet energy level of the antenna only changed slightly with the substituent groups of the biphenyl backbone (vide infra), we exclude the possibility that the quenching of luminescence is due to a change of the nature of the antenna triplet state. It is well-known that the O−H oscillator of the solvent coordinated to the metal center can provide an efficient nonradiative path,[29] so these observations of the relatively low luminescence performances of complexes with L^{II} may be related to the presence of solvent in the inner coordinated sphere of lanthanide centers, which is in perfect consistent agreement with the proposed structural results.

Compared with the emission spectra of the four complexes with either L^I or L^{II} (Table 3), the transition intensity follows the trend $Tb^{3+} > Dy^{3+} > Eu^{3+} > Sm^{3+}$, which means that the energy transfer from the organic ligands to Tb^{3+} and Dy^{3+} is more effective than that to Eu^{3+} and Sm^{3+}. This behavior can be rationalized by the ligand-to-metal energy transfer discussed below.

Energy Transfer between the Ligand and Ln^{3+}. In the energy transfer from the ligand to the metal, the triplet-state energy of the ligand is regarded as an important factor in the excitation of the lanthanide cation.[30,31] In order to acquire the triplet-state energy levels (T_0) of ligands L^I and L^{II}, the low-temperature (77 K) phosphorescence spectra of the Gd^{3+} complexes of L^I and L^{II} were measured in a 1:1 methanol-ethyl acetate (v/v) glassing solvent, shown in Figures S10 and S11 (Supporting Information). From the phosphorescence spectra, the triplet energy levels (T_0) of the Gd^{3+} complexes, which correspond to their lower wavelength emission edges, are 23 474 cm^{-1} (426 nm) and 22 935 cm^{-1} (436 nm). Because the lowest excited state, $^6P_{7/2}$ ($E(^6P_{7/2}) = 32\,000$ cm^{-1}) of Gd^{3+} is much higher than the lowest-lying triplet levels of most chromophores, the data obtained from the phosphorescence spectrum actually reveal the triplet energy level of the ligand in lanthanide complexes. Latva et al.'s empirical rule[32,33] states that an optimal ligand-to-metal energy transfer process for Ln^{3+} needs ($\Delta E = E(T_0) - E(^5D_J)$) 2500−4000 cm^{-1} for Eu^{3+} and 2500−4500 cm^{-1}

(28) Kirby, A. F.; Foster, D.; Richardson, F. S. *Chem. Phys. Lett.* **1983**, *95*, 507–512.

(29) Horrocks, W. D.; Sudnick, D. R. *J. Am. Chem. Soc.* **1979**, *101*, 334–342.

(30) Bhaumic, M. L.; El-Sayed, M. A. *J. Phys. Chem.* **1965**, *69*, 275–280.

(31) Dawson, W.; Kropp, J.; Windsor, M. *J. Chem. Phys.* **1966**, *45*, 2410–2418.

for Tb^{3+}. The experimentally observed T_0 energy levels of ligands L^I and L^{II} are ca. 3074 and 2535 cm^{-1} higher than the $^5D_4$ level of Tb^{3+} (20 400 cm^{-1}), and ca. 2474 and 1935 cm^{-1} higher than the $^4F_{9/2}$ level of Dy^{3+} (21 000 cm^{-1}), respectively, which facilitates efficient energy transfer. By contrast, the lowest-energy Eu^{3+} and Sm^{3+} acceptor levels are at 17 300 ($^5D_0$) and 17 900 cm^{-1} ($^4G_{5/2}$), both of which are significantly lower in energy than the T_0 energy levels of the two ligands. This therefore supports the observation of stronger sensitization of the terbium and dysprosium complexes than the europium and samarium complexes because of the larger energy gap between the ligand triplet and the europium or samarium ion excited states.

Conclusions

This study demonstrates that the flexible exo-bidentate ligands derived from biphenol featuring two benzylsalicylamide arms, 2,2′-bis{[(2′-benzylaminoformyl)phenoxyl]ethoxyl}-1,1′-biphenylene (L^I) and 5,5′-dibromo-2,2′-bis{[(2′-benzylaminoformyl)phenoxyl]ethoxyl}-1,1′-biphenylene (L^{II}), form interesting structures with lanthanide cations via the carbonyl oxygen donors. The two structurally related ligands with different coordination conformations can both function as bridging linkers to generate novel lanthanide coordination polymers with diverse frameworks, which are distinctly different from those in our previous report. It is obvious that replacement of the two hydrogen atoms by two bromine atoms in the 5- and 5′- positions of the biphenyl backbone significantly affects the conformational distortion of the nonplanar ligand, which considerably changes the overall frameworks from two-dimensional honeycomb-like (6,3) topology nets to one-dimensional single-stranded helical chains. Luminescence studies also demonstrate that the two salicylamide-based ligands exhibit a good antenna effect for Ln^{3+} cations and provide excellent sensitization of the Tb^{3+} luminescence through a particularly efficient ligand-to-lanthanide energy transfer process. On the other hand, the photophysical properties of the lanthanide complexes can also be fine-tuned by changing the substituents on the biphenyl backbone, which have significant influence on coordination behavior. All of these results reveal that the conformational distortion of the nonplanar flexible ligand can be tuned through slight structural modification. And the change of conformational distortions of nonplanar flexible ligands has a profound effect on determining the coordination environments of the metal centers and, consequently, the topologies of the frameworks as well as luminescence properties.

Supporting Information Available: Materials and instrumentation, CIF files, tables of interatomic distances and angles for **1**−**4**, synthetic procedure for ligands and their lanthanide complexes, XRPD patterns of the Tb^{3+} complex with L^I and the Dy^{3+} complex with L^{II}, absorption spectra of ligands L^I and L^{II}, the room-temperature solid-state emission spectra for the Sm^{3+} and Dy^{3+} complexes with L^I, phosphorescence spectra of the Gd^{3+} complexes with L^I and L^{II}, the room-temperature solid-state phosphorescence lifetimes of the Eu^{3+} and Tb^{3+} complexes with L^I and L^{II}. This material is available free of charge via the Internet at http://pubs.acs.org.

Acknowledgment. The authors acknowledge financial support from the National Natural Science Foundation of China Research (Grants 20771048 and 20621091).

IC802060E

(32) Latva, M.; Takalo, H.; Mukkala, V.-M.; Matachescu, C.; Rodriguez-Ubis, J. C.; Kankare, J. *J. Lumin.* **1997**, *75*, 149–169.
(33) Arnaud, N.; Georges, J *Spectrochim. Acta, Part A* **2003**, *59*, 1829–1840.